scientific reports

Check for updates

OPEN

Sustainable engineering of fiber-reinforced geopolymer-treated low plasticity clay linking geomechanics and microstructure through support vector machines

Mazhar Syed[1], Mohammed Ashfaq[2], Babak Jamhiri[3], Umair Ali[1,4]✉ & Fazal E. Jalal[1]✉

The variations in soft soil exhibiting low plasticity often damage lightweight structures, costing billions annually. Although well-known traditional stabilizers are efficacious, their production can have a massive environmental impact. This paper investigates the geomechanical efficiency of low-plasticity clay reinforced with chemically treated banana fiber (CTBF) and EnviroSafe geopolymers, comprising alkaline solutions and industrial waste materials. The proportions of coal gangue ash (CGA) replacement with silica fume (SF: 0–20%) were varied in the alkaline solution by maintaining a 0.4 water-to-solid ratio. A series of consolidation, compression, shear, and penetration resistance tests were performed to determine the geomechanical properties. In addition, Stereoscopic, Fourier-transform infrared (FTIR) spectroscopy, and Thermogravimetry analysis (TGA) tests were conducted at varying CTBF-SF mixture dosages. The study demonstrated a substantial improvement in the strength characteristics of CGA-SF in geopolymer-stabilized low-plasticity clay. The results of SF (> 10%) in CGA-based geopolymer stabilizer soil attained the lowest equilibrium void ratio over the unreinforced soil. Furthermore, a support vector machine (SVM) algorithm model was proposed to predict the geomechanical strength of fiber-reinforced alkaline soil, and the results showed an excellent predictor of geomechanical strength performance.

Keywords Low-plasticity clay, Banana fiber reinforcement, Alkaline activated material, Shear strength ratio, Support vector model

Poor mechanical properties and inadequate load-bearing capacity of the infrastructure resting on soft ground are significant concerns in geotechnical engineering. Because of the swift development of infrastructure, it is extremely challenging to deal with different clays having fluctuating characteristics during the construction phase, which generally includes a variety of problematic soils (i.e., soft, swell-shrink, hydrophilic, liquefiable, acid sulfate, peaty, saline, organic, collapsible soils, among others)[1–3]. Of these, the low-plasticity clays generally exhibit high natural moisture content[4], high compressibility[5], strong rheological characteristics[6], weak permeability and low shear strength[7], high natural permeability and poor load-bearing capacity[8], which leads to a multitude of problems in the form of uncontrolled distortion as well as structural instability[2,9]. These soils are broadly distributed throughout the globe in more than 40 countries. Their properties are mainly governed by both macro-factors (i.e., surcharge, water drainage circumstances, consolidation time, and depth), as well as micro-factors, such that the complex characteristics serve as the concentrated representation of their microstructural properties[10]. Such soils are detrimental to civil engineering structures and require treatment using various stabilizer materials. Nowadays, the non-traditional nano-chemical stabilization is superior to conventional stabilizing techniques owing to its cost-effectiveness and enhanced environmental conservation[11–14]. The worldwide increase in greenhouse gas emissions has been primarily attributed to the utilization of fossil fuels at the gross level for power generation and domestic purposes[15,16]. Within the context of coal mining

[1]Interdisciplinary Research Centre for Construction and Building Materials, King Fahd University of Petroleum and Minerals, Dhahran 31261, Saudi Arabia. [2]Technical Manager, Osaimi Geotechnic Company, Al Khobar 31952, Saudi Arabia. [3]School of Architecture, Building and Civil Engineering, Loughborough University, Loughborough, UK. [4]Department of Civil and Environmental Engineering, King Fahd University of Petroleum & Minerals, Dhahran 31261, Saudi Arabia. ✉email: syed.naqvi@kfupm.edu.sa; fazal.jalal@kfupm.edu.sa

wastes, coal gangue (CG) is considered a heterogeneous waste produced during the mineral processing or coal cleaning phase of the mining process. It is noteworthy to mention that millions of tonnes of CG are recorded to be stockpiled (≈ 20–40% of the entire mining waste) at different coal mines on a global scale. Asian regions, especially China's substantial coal production, reaching 4.13 billion tons in 2021, have led to a significant increase in CG production (743 million tons, representing a 5.84% rise). Additionally, the cumulative storage of CG approaches approximately 7 billion tons (i.e., almost 6.79% of China's arable land) from more than 2,000 gangue hills that cover around 200,000 mu. It is also pertinent to mention that the annual growth rate exceeds 800 million tons. The substantial accumulation poses a serious environmental and land-use challenge. Various researchers have proved the successful utilization of CG in geotechnical applications, especially in expansive soil[17–20]. Wang et al.[21] examined the influence of various alkali activators on the strength and microstructure of geopolymers formed from CG calcined at 700˚C. NaOH concentrations, liquid-solid ratios, and Na_2SiO_3/NaOH ratios were varied, and achieved the rapid improvement in shear strength and compactness of the geopolymer under optimal activator. The inclusion of fines to CG changes its gradation from poorly graded sand to silty sand. Also, the geotechnical indices of the CG depict its potential application in the form of fill material. The presence of silica and alumina imparts a pozzolanic nature to CG, whereas quartz and kaolinite render it a suitable geomaterial. In addition, its California Bearing Ratio (CBR) value, as well as its collapse behavior, also guarantee that it can be employed as subgrade material[15,22]. Moreover, the carbon footprint assessment (CFA) on CG applications reveals a substantial reduction in carbon emissions. For instance, these emissions are reduced by 3210 kg CO_2e/m^3 (in case of embankment construction in contrast to traditional fill materials), 1709 kg CO_2e/m^3 (in case of mechanically stabilized earth wall), 1168 kg CO_2e/m^3 (in case of plain embankments), 14.4 kg CO_2e/m^3 (in case of reinforced earth walls), and 135.4 kg CO_2e/m^3 (in case of subbase material)[23–25].

It is imperative to mention that various machine learning (ML) tools or AI techniques, especially in geo-environmental engineering, are found to be immensely reliable and practical tools to solve complex problems with perplexed dynamics[26,27]. In this context, the addition of CG to expansive black cotton (BC) soil revealed that CBR values decrease beyond 40% CG due to reduced cohesion. However, the inclusion of CaO ameliorated the CBR values, with the 6CaO and 40CG combination showing superior performance[28]. While predicting the UCS and CBR of chemically treated CG with the help of ANN and random forest (RF) approaches, Ashfaq et al.[29] found that the UCS of CG exhibited an increasing trend when the CaO amount, gypsum content, and CP were increased. Note that the maximum value of 1,050% was obtained for 1.5% gypsum and 6% CaO inclusion. In yet another study by Amin et al.[30], the neural network-based models demonstrated strong performance with *R* values of 0.993, 0.995, and 0.997 for UCS, unsoaked CBR, and soaked CBR, respectively. Furthermore, both the CBR and UCS witnessed a significant increase when stabilizer content was incorporated, thereby surpassing those of untreated low-plasticity clay (CBR = 3.862 and UCS = 0.8097) that met the construction standards (Krishna et al., 2023). Compared to the other learners, for instance, ANNs, the support vector machine (SVM) approach provides an improvement in the functionality because it usually achieves a better learning convergence with a simpler search optimization[31], whereas ANNs can get stuck in local extrema without a proper optimization[32,33]. Given tree-based models, such as regression trees or Random Forests (RF), SVMs exhibit better abilities to comprehend the non-linearity among variables. Also, SVMs exhibit good generalization performance suitable for tasks where the model needs to perform well on unseen data. However, like other machine learning models, these models require hyperparameter tuning when developing predictive models. The tuning can be done manually by repeatedly changing settings. On the contrary, SVMs have shown great compatibility with hyperparameter optimization methods, which render them even more of a viable option for developing ML-based predictive models[34,35].

The present study primarily focuses on utilizing residual industrial waste in alkali-activated material as a smart, sustainable, and cost-effective soil stabilizer. This study aims to improve the geomechanical behavior of low-plasticity clay through geopolymerization, utilizing chemically treated banana fiber (CTBF) as a reinforcement material under varying coal gang ash-silica fume proportions. The research also analyzes a series of microstructural and geotechnical behavior tests on CTBF, CG ash, silica fume (i.e., CTBF-CGA-SF)-based geopolymer soil. To the best of our knowledge, the existing literature does not cover the CBR and UCS of CG-stabilized low-plasticity clays using the SVM method. Although past studies have utilized various AI tools for predicting CBR values, they face limitations such as sensitivity to hyperparameters and a lack of interpretability. The current study aims to overcome these constraints, thereby providing an enhanced prediction model that is essential for informed decision-making across various applications.

Material properties

Low-plasticity clay

For this investigation, low-plasticity clay was taken from a site located in Telangana's Nalgonda district. The collection involved disturbed samples extracted from a shallow depth of nearly 15 centimeters below ground level. According to the classification criteria outlined in the Unified Soil Classification System (USCS), the soil type is classified as Intermediate Compressible Clay (CI), containing approximately 55% fine-grained material. The acquired soil samples exhibited a semi-black appearance and contained a substantial amount of clay loam. Before use, these soil samples were pulverized and subsequently subjected to a 24-hour drying process at around 105 °C. Moreover, this type of clayey soil, commonly found in Telangana, is renowned for its problematic characteristics, particularly its behavior regarding moisture content and compressibility. In-situ measurements using a rapid moisture meter revealed a high soil moisture content accompanied by low shear strength.

Coal gangue Ash and silica fume

Coal Gangue Ash (CGA) and Silica fume (SF) used in this study were sourced from Bhupalpally Singareni Collieries, Telangana, and Jindal South-West (JSW) Cement Limited, Vishakhapatnam, respectively. Both CGA

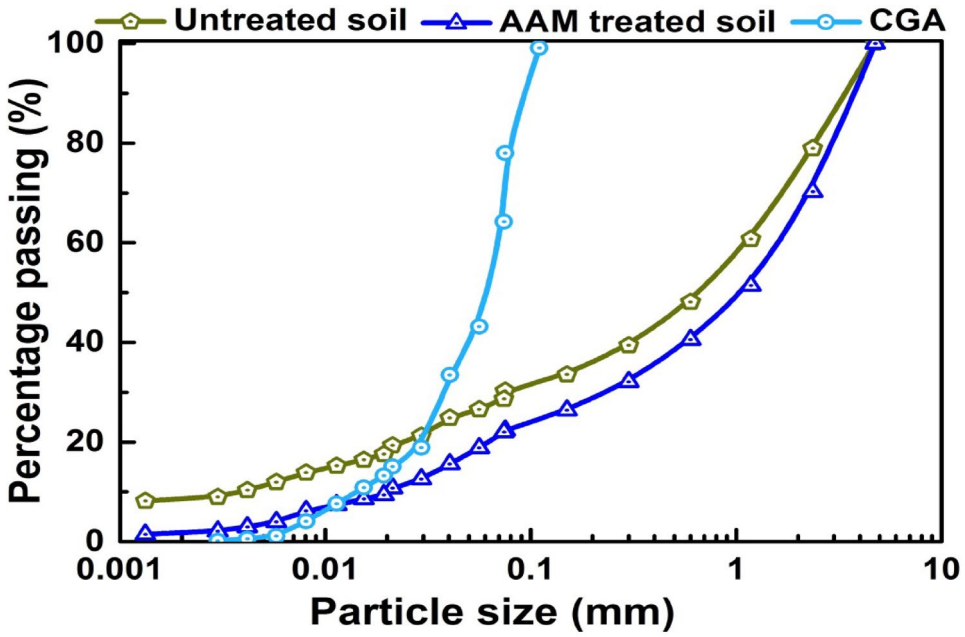

Fig. 1. Particle size analysis of materials.

Properties	Low-plasticity clay	CGA	SF	Parameter	UBF
pH	7.9	7.18	11.5	Diameter (μm)	38
Specific gravity	2.5	2.51	2.5	Specific gravity	0.88
Swelling Index (%)	78	19	-	Tensile strength (MPa)	125
Liquid limit (%)	42	28	-	Elastic modulus (MPa)	3250
Plasticity index (%)	29	-	-	Cellulose (%)	58
Dry unit weight (g/cc)	1.7	21	2.4	Hemicellulose (%)	16
Water content (%)	21	17.5	-	Lignin (%)	10
UCS (kPa)	198	-		Ash (%)	3
Indirect tensile strength (kPa)	24	-		Wax (%)	1
Soaked CBR (%)	2.28	-	-		
Swelling pressure (kPa)	68	-	-		

Table 1. Engineering properties of clayey soil, CGA, SF, and fiber materials.

and SF employed in this study conform to ASTM C618[36] and ASTM C989[37]. These materials were used as dry precursors in the preparation of the alkaline binder. Figure 1 illustrates the particle size distribution curves for CGA, untreated soil, and the geopolymer-stabilized subgrade soil. A detailed summary of the engineering properties of the constituent materials is presented in Table 1.

Fiber treatment

Untreated banana fibers (UBF), with lengths ranging from 20 to 30 mm and diameters less than 33 μm, were procured from Go-Green Industries, Tamil Nadu. The dimensional attributes of the fibers—particularly their length and diameter are recognized as critical factors influencing their effectiveness in soil reinforcement applications. Many researchers have demonstrated that natural fiber lengths between 20 mm and 40 mm can effectively resist higher friction and mobilization, as well as interfacial bonding, under low desiccation and soil surface cracking conditions[38,39]. Hence, in the present research, fiber lengths between 20 and 30 mm were selected as an optimum length in AA-stabilized soil. Moreover, before reinforcing the banana fiber in the soil mixture, the fiber was chemically treated with calcium hydroxide ($Ca(OH)_2$) to delay the degradability and serviceability. A step-by-step procedure for treating fibers is shown in Fig. 2. Initially, the raw banana fibers were immersed in water for 24 h, followed by boiling for 30 min to remove waxy coatings and reduce the presence of natural oils on the fiber surface. The dried fibers were then placed in a 1000 mL solution of $Ca(OH)_2$ (12 Molarity) for seven days, facilitating thorough absorption of the solution into the fiber matrix. After treatment, the fibers were rinsed with clean water to eliminate any remaining calcite deposits. Finally, the processed fibers were dried at a controlled temperature of 23 ± 2 °C for seven days. The chemical composition of low-plasticity clay, CGA, SF, and both untreated banana fiber (UBF) and CTBF is provided in Table 2.

Fig. 2. Chemical treatment process of banana fiber.

Elements (%)	Low-plasticity clay	CGA	SF	UBF	TBF
SiO_2	23.40	51.20	85.20	1.86	1.30
Al_2O_3	5.12	26.10	3.60	0.30	0.0
CaO	4.60	2.10	1.10	20.50	45.60
K_2O	2.70	1.80	0.89	0.80	2.30
MgO	7.96	0.70	1.01	0.10	0.00
P_2O_5	1.60	0.20	0.08	1.50	4.30
Na_2O	44.65	0.14	0.81	70.20	20.10
Cl	0.60	0.06	0.65	1.30	2.40
SO_3	0.20	0.05	1.16	1.30	3.50
FE_2O_3	4.90	2.60	0.50	0.30	7.10

Table 2. Chemical composition of clayey soil, CGA, SF, UBF, and TBF.

Sample	Mass of Geopolymer Components per Unit Volume of Subgrade Soil (kg/m³)					
	geopolymer	CGA	SF	NaOH	Na_2SiO_3	H_2O
$SA_6C_{100}F_0$	102.42	62.57	0.00	1.65	20.28	17.98
$SA_6C_{95}F_5$	102.42	59.44	3.12	1.65	20.28	17.98
$SA_6C_{90}F_{10}$	102.42	56.31	6.25	1.65	20.28	17.98
$SA_6C_{85}F_{15}$	102.42	50.06	12.51	1.65	20.28	17.98
$SA_6C_{80}F_{20}$	102.42	43.80	18.77	1.65	20.28	17.98

Table 3. Required quantities of geopolymer for subgrade soil with varying CGA–SF Ratios.

Alkali-activated materials or geopolymer preparation

Alkali-acActivated materials (AAM) were prepared by mixing CGA and SF with an aqueous alkaline activator solution. The activator was prepared by maintaining a mass ratio of 280:129.43:120:10.57[40] for CGA, sodium silicate (Na_2SiO_3), SF, and sodium hydroxide (NaOH), respectively. The solution was produced by combining crushed NaOH pellets with a liquid Na_2SiO_3 solution, both procured from Hychem Laboratories, Hyderabad, India. The Na_2SiO_3 solution contained around 30% silicon dioxide (SiO_2), 15% sodium oxide (Na_2O), and 54% water (H_2O). To obtain the optimal geopolymer composition, CGA and SF were blended in varying proportions, with CGA ranging from 100% to 80% and SF from 0% to 20%. Table 3 presents the dosage of alkaline binder required per cubic meter of low-plasticity clay for each CGA–SF mixture.

Sample mixing and curing

The geopolymer paste was uniformly blended with low-plasticity clay using different combinations of CGA: 80–100% and SF: 0–20%, maintaining a moisture-to-solid ratio of 0.4 in the alkaline activator. The geopolymer dosages of 1%, 3%, 6%, and 10% (based on the dry weight of soil) were initially evaluated for soil stabilization before fiber reinforcement. To minimize data clustering, a 6% geopolymer binder was selected as the optimal stabilizer, incorporating CGA–SF ratios of 100:0, 95:5, 90:10, 85:15, and 80:20, respectively, based on cost efficiency, workability, alkali reactivity, binding capacity, and shrinkage resistance. Various CTBF reinforcement dosages were mixed into the geopolymer-treated soil and covered with dampened jute sheets, allowing curing under ambient conditions for 28 days. After curing, the CTBF–geopolymer soil composites were subjected to detailed microstructural and geotechnical testing. Table 4 presents the terminology used for CTBF–CGA–SF -based geopolymer-stabilized soil.

Methodology

Microstructural characterization

Microstructural investigations—including stereomicroscopy, Fourier-transform infrared (FTIR) spectroscopy, and thermogravimetric analysis (TGA)—were performed on untreated banana fiber, CTBF, and low-plasticity clay stabilized with CGA–SF-based alkali-activated mixtures. Surface topography of the soil was examined using a stereo microscope (Olympus SXZ7) operated at various magnifications (1×, 2.5×, 4.5×, and 5.6×), with a resolution capability of up to 20 µm. Molecular bond transmittance was analyzed using a potassium bromide (KBr) pellet-based FTIR spectrometer (JASCO-4200). Spectral data were recorded across a wavenumber range of 4000–500 cm^{-1} for both fiber and geopolymer-stabilized soil matrices. In addition, thermal degradation behavior was evaluated through thermogravimetric analysis using a Shimadzu DTG-60 analyzer, applying a controlled heating rate of 10 °C/min to approximately 15 mg of sample under a nitrogen atmosphere, with temperature reaching up to 800 °C.

Geotechnical characterization

A series of soil behaviour and mechanical strength testing, including consolidation, compression, and penetration resistance, was performed on geopolymer-stabilized soil, and CTBF-reinforced geopolymer composites containing varying proportions of SF-CGA. The relationship between void ratio (e) and effective stress (σ) was examined using a 3-cell consolidometer setup in accordance with ASTM D2435. Both untreated and treated specimens were sandwiched between porous stone in a consolidation ring of 6 cm diameter and 2 cm thickness. Measurements of sample height and percentage swelling were recorded at 24-hour intervals under a preload of 6.5 kPa, with loading continued until a peak effective stress of 800 kPa was achieved.

The unconfined compressive strength (UCS) of the soil was evaluated by preparing soil–fiber composite specimens within cylindrical molds of 3.8 cm diameter and 7.6 cm height. Load was applied using a strain-controlled compression testing apparatus with a maximum capacity of 20 kN, operated at a constant strain rate of 1.25 mm/min. The improvement in shear strength due to fiber addition was quantified using the shear strength ratio (CSR), expressed in Eq. (1), which represents the ratio of UCS (kPa) for fiber-reinforced (i.e., CTBF) soil to that of unreinforced soil.

$$CSR = \frac{UCS_{(CTBF=0.25,\ 0.5,\ 0.75,\ 1\%)}}{UCS_{\ ZeroCTBF}} \tag{1}$$

Penetration resistance of CTBF-geopolymer stabilized soil containing SF and CGA was evaluated using the CBR method under a 15 cm diameter cylindrical mold. The compacted CTBF-soil composite specimens were submerged in water for 4 days, and penetration was applied using a 5 cm diameter plunger at a constant strain rate of 1.25 mm/min. Additionally, the subgrade resilient modulus (M_R) (MPa) was determined from the corresponding CBR values (%) using Eq. (2), in accordance with the guidelines provided in IRC:37[41]:

$$M_R = 17.6 \times (CBR)^{0.64} \tag{2}$$

Support vector-based modelling

SVMs have demonstrated strong effectiveness in addressing high-dimensional problems involving function approximation, feature selection, classification, and predictive modeling. It is pertinent to mention that SVMs are advantageous due to their efficacy in high-dimensional spaces, robustness in dealing with the problem of overfitting, adaptable kernel functions, and improved performance in cases of small datasets. However, some of their main limitations include being computationally expensive, sensitivity to parameter tuning,

Combination	Sample definition
All percentages of Coal Gangue ash and Silica fume were kept at 100% in the geopolymer paste.	$SA_6\ C_xF_y$: Binder prepared with various %age of geopolymer
Mixing of geopolymer paste into the soil at 1, 3, 6, and 10%	S = Low-plasticity clay F = Silica fume A = AAM/geopolymer C = Coal Gangue ash x=% of coal gangue ash (100, 95, 90, 85, and 80%) y=% of Silica fume (0, 5, 10, 15, and 20%)
geopolymer-treated soil cured for a 28-day curing period	$SA_6\ C_{100}F_0$ $SA_6\ C_{95}F_5$ $SA_6\ C_{90}F_{10}$ $SA_6\ C_{85}F_{15}$ $SA_6\ C_{80}F_{20}$

Table 4. Sample mix definition for CTBF-CGA-SF stabilized soil.

lower transparency, and limited efficiency with noisy datasets. It is essential to recognize that the benefits and drawbacks of SVMs can vary depending on the specifics of the challenge and the dataset available when employing SVM-based modeling to evaluate the strength characteristics of fiber-reinforced CG. As a result, it is highly recommended to conduct extensive testing with various algorithms and evaluate their performance before deciding on the best strategy for a given scenario. Furthermore, leveraging its kernel type, the SVM approach proves to be a powerful machine learning model that can effectively substitute traditional regression analyses. The SVM model can be mathematically represented as Eq. 3.

$$\hat{y}_i = w^T \psi\ (x_i) + b \tag{3}$$

where $\psi(x_i)$ stands for a kernel function that maps the input data to a desired linear or nonlinear feature space, w^T denotes the weight vector, and b refers to the intermediary coordinate of the regression hyperplane. Although SVMs can classify and predict based on the predictive model, the type of kernel functions, as well as their hyperparameters, both affect the final accuracy. Therefore, it is important to develop predictive models by incorporating the optimized hyperparameters. Note that there are several optimization methods, such as (i) search-based methods (i.e., random search and grid search)[31] and (ii) (meta)heuristic methods (i.e., evolutionary and population-based methods)[34]. Further details about the evolutionary hyperparameter optimization of ML methods can be found in Chen et al.[42].

This study employs three types of baseline models: the plain SVM with manual settings, Grid search-based SVM (GS-SVM), and genetic algorithm-optimized SVM (GA-SVM), to ensure the validity of predictions. Hence, a variety of hyperparameter optimizations are employed, which also allows for the comparison of the prediction power of the developed models. Moreover, it is imperative to effectively refine the experimental observations of bias, missing observations, and multicollinearity before developing the predictive models. Accordingly, three predictive input parameters, namely, CGA, SF, and BF, were adopted to predict the response behaviour of two output variables (i.e., UCS and CBR). Consequently, Figs. 3 and 4 illustrate the pairwise relationships among variables, along with their statistical distributions. These pairplots are effective for exploring the relationships between variables in the dataset and identifying trends in variables. As shown in the aforementioned figures, the diagonal histograms display the marginal distributions, and the remaining graphs illustrate the pairwise correlations. Based on the experimental observations, Figs. 3 and 4 suggest that, with increasing BF and SF, the strength characteristics (CBR and UCS) decrease. In contrast, the CGA increases, leading to reduced UCS and CBR values. Considering the pairs of variables, the experimental observations also suggest the existence of a negative correlation between SF and CGA. Hence, SF is inversely related to CGA. However, there is no tangible correlation between the three input attributes. These observations indicate that the effects of SF and CGA can be correlated, while BF does not correlate with other input variables. Noticeably, the effects of input variables on the predicted strength characteristics can be identified later based on the predictive SVM models. Noticeably, 225 entries of experimental observations have been incorporated into two portions to formulate the SVM-based

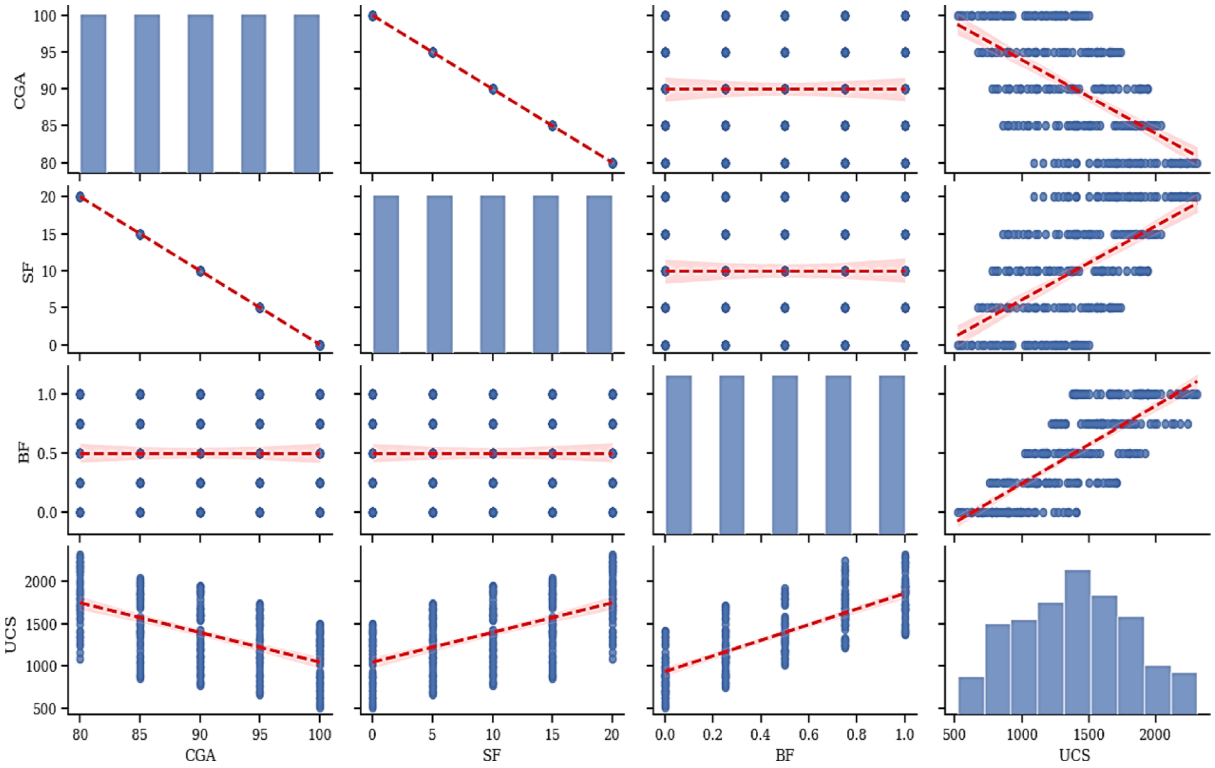

Fig. 3. Pair plots of statistics, correlation among input/output variables while processing the UCS dataset.

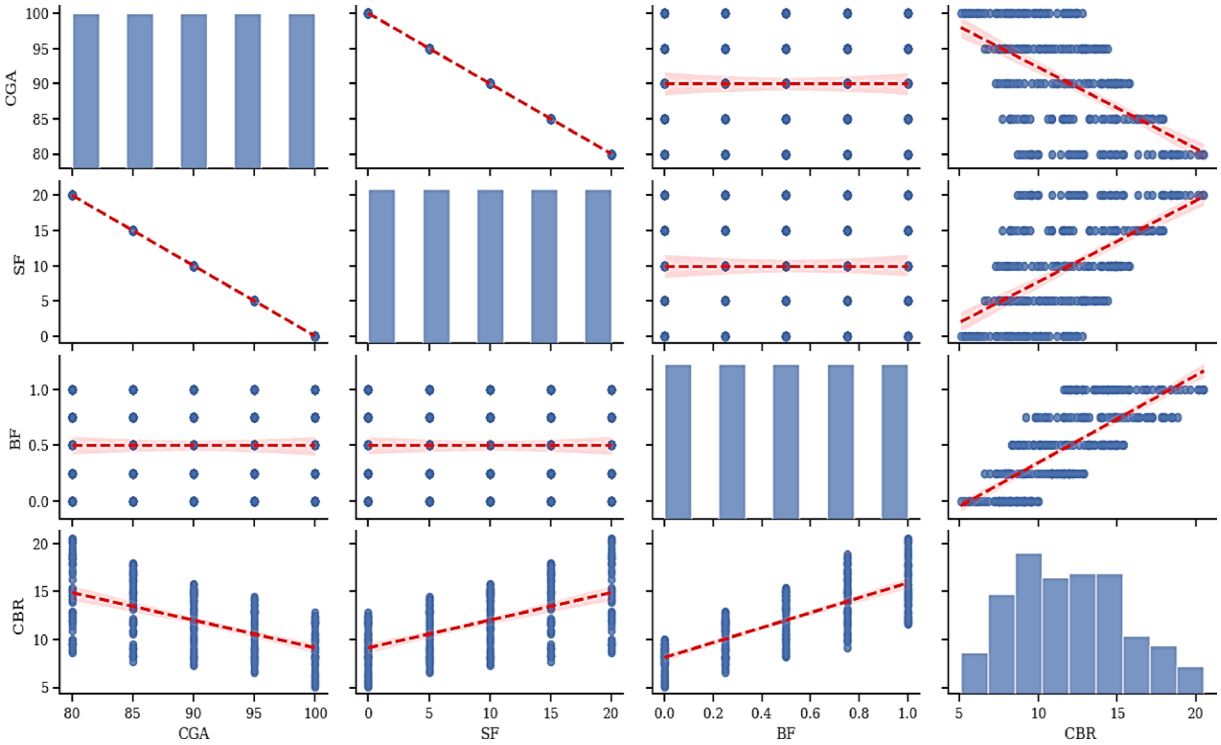

Fig. 4. Pair plots of statistics, correlation among input/output variables while processing the CBR dataset.

models. After splitting the data randomly, 80% of the entries were used for training the models, whereas the remaining portion was used to test the predictions. These predictive models help to identify the influential variables on the prediction outputs (i.e., UCS and CBR).

SHAP (SHapley additive exPlanations) analysis

To move beyond predictive accuracy and understand how the input variables influence the model's output, we employed SHAP (SHapley Additive exPlanations). SHAP is a state-of-the-art method from cooperative game theory used to explain the output of any machine learning model. It provides a unified framework for model interpretation, offering both consistency and local accuracy. The core of SHAP is the Shapley value, which represents the average marginal contribution of a feature value to the prediction across all possible feature combinations. For each prediction, SHAP assigns an importance value to each input feature, indicating its contribution to pushing the model's output from the base value (the average prediction over the training dataset) to the final predicted value. This allows for a detailed understanding of both global interpretability by aggregating the Shapley values for each feature across all data points, determining the overall importance and influence of each variable (CGA, SF, and BF) on the geomechanical properties (UCS and CBR). The local interpretability of SHAP can explain why a single, specific prediction was made, offering insight into the model's behavior for individual samples. The flowchart in Fig. 5 illustrates the complete workflow of the support vector regression modeling process used in the study. It begins with a dataset of 225 experimental observations that undergo data preprocessing, including data splitting and feature scaling. The optimized model is then developed using genetic algorithm and grid search approaches, followed by model testing, performance evaluation, and interpretability analysis using SHAP, ensuring both predictive accuracy and transparency in model behavior.

Results and analysis

Microstructural characterization

Stereomicroscopic images

A series of microscopic surface images of low-plasticity clay is collected by using a stereomicroscope under varying magnifications. Figure 6(a-d) illustrates the typical stereomicroscopic images for untreated low-plasticity clay, soil mixed with an alkaline binder, and geopolymer soil reinforced with fibers at varying CGA-SF content. Figure 6(a) illustrates areas of yellowish and light brown pigmentation in the untreated low-plasticity clay, which may be interpreted due to the presence of illite-smectite and iron groups. Additionally, irregular surface cracks are visible on the untreated soil, which will significantly impact the volumetric behavior when the water level fluctuates. Figure 6(b) shows a thin layer of hardened geopolymer paste deposition around the cracks of the clay matrix. The bright and shiny regions may be due to the presence of mica from the SF. In contrast, the dark black colored patches are voids caused by early moisture evaporation from the solidified alkaline binder. The randomly distributed CTBF in the CGA-based geopolymer soil combination at 0 and 20% SF content is depicted in Figs. 6(c-d). Moreover, the morphology of CTBF reinforcement in the soil matrix has formed a spatially

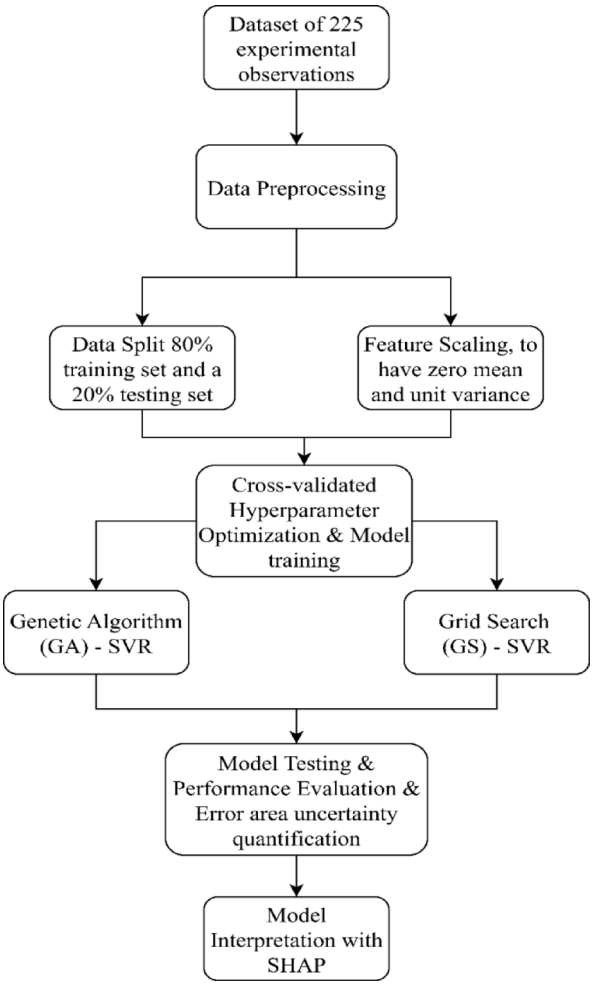

Fig. 5. Schematic representation of the Support Vector Machine (SVM) workflow used in this study, including data preprocessing, kernel optimization, model training, testing, and SHAP-based interpretability analysis.

grooved network, which relatively enhances interlocking friction by restricting the clay. particles during load application. Adding CTBF is beneficial as it strengthens the interfacial bonding, resulting in higher tensile and frictional resistance. As a result, the combined action of CTBF, CGA, and SF improves the load-bearing capacity and stiffness of geopolymer-stabilized soil, attributed to the development of an active pozzolanic matrix.

Fourier transform infrared (FTIR) spectroscopy

FTIR spectra for banana fiber before and after chemical treatment, untreated low-plasticity clay, and geopolymer stabilized soil at various CG and SF dosages are shown in Figs. 7(a-b). The molecular bonding curves of untreated banana fibers (Fig. 7a) are characterized by hydroxyl O-H stretching at around 3300 cm^{-1}, mostly due to the presence of cellulose and water. Moreover, the untreated soil in Fig. 7(b) shows a sharp band of Portlandite [$Ca(OH)_2$] at 3600 cm^{-1}. The broadband of O-H water stretching (3600 cm^{-1}) and C-H alcohol (3400 cm^{-1}) was reduced in both CG (100%) and SF (20%) based geopolymer treated soil relative to untreated soil. Also, the C-H methyl group at around 2950 cm^{-1} showed the same peaks before and after chemical treatment of fibers[43]. The C = O carbonyl functional group is not apparent at 2900 cm^{-1} as the replacement of CG with SF increases in the geopolymer mixed soil. The pozzolanic reaction in silica-rich soil roughly characterizes this spectrum. The transmittance spectra for geopolymer-treated soil containing high CGA (100%) show the marginal peak of the = CH2 bond compared to SF (20%) based geopolymer-treated soil. These modifications in soil chemical structures due to carbonation may be associated with minimal chemical weathering reactions on the clay surfaces[44]. Interestingly, the symmetric stretching vibration of Si-O at 1030 cm^{-1} remains identifiable even after the chemical treatment of fibers[45]. A sharp characteristic band of Si-Al-O at 800 cm^{-1} was observed in the untreated soil and the geopolymer mixed soil. Apart from that, the Si-O plane stretching vibration was identified in the range of wavenumbers around 580 cm^{-1}. Thus, with a chemical shift of roughly 10–20 cm^{-1}, the transmittance peaks from untreated fibers and geopolymer-treated soil reveal identical linkages.

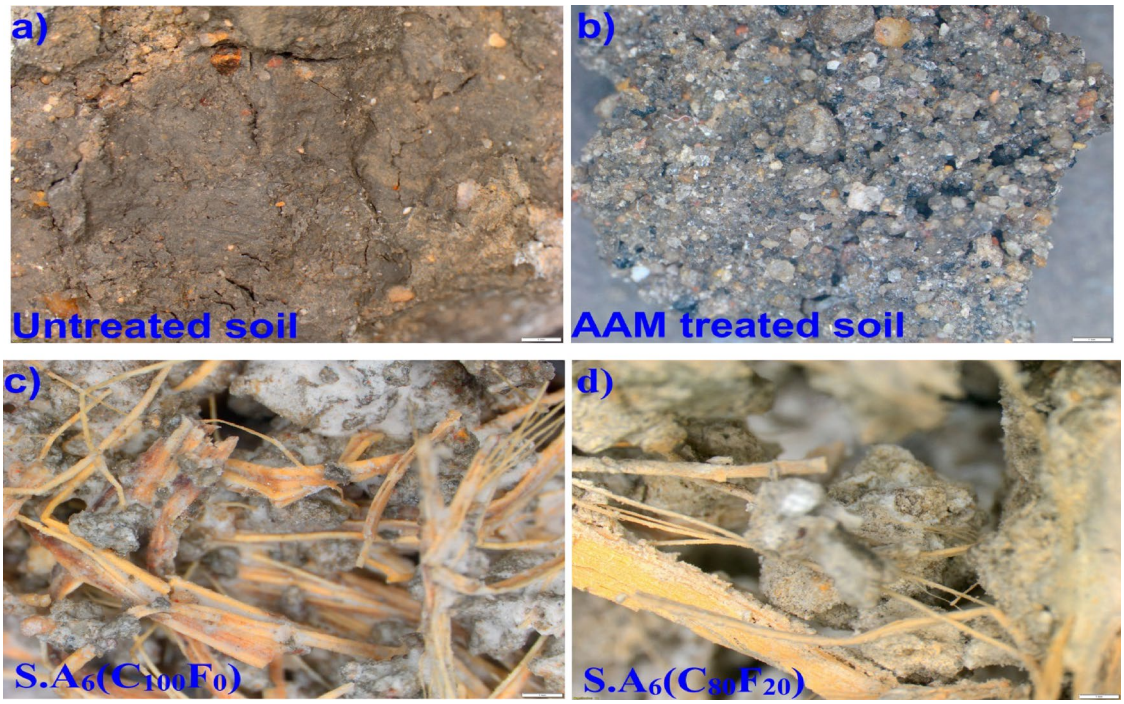

Fig. 6. Stereomicroscopic images of **(a)** untreated soil, **(b)** geopolymer-soil, **(c)** CGA-based geopolymer-CTBF soil, **(d)** SF-CGA-based geopolymer-CTBF reinforced soil.

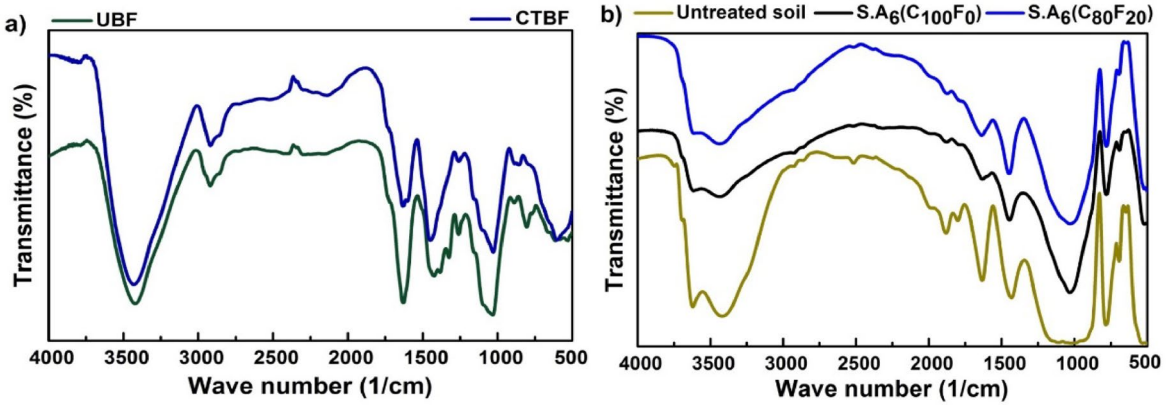

Fig. 7. FTIR curve of UBF and CTBF **b)** Raw and geopolymer-treated soil.

Thermogravimetric analysis (TGA)

Thermogravimetric (TG) and derivative thermogravimetric (DTG) analysis are used to calculate the stability of compounds and mass fractions against temperature. Figure 8 displays the TGA/DTG profiles of UBF and CTBF, focusing on mass reduction and its first derivative. An initial drop in mass was observed for both UBF and CTBF samples between 100 and 150 °C, likely resulting from rapid evaporation of free water within the fiber matrix[46]. The mass loss in UBF was found to be relatively higher (4–5%) than in CTBF, which may be attributed to a greater decomposition rate of volatile components in the untreated fibers. Additionally, the TG/DTG trends for both UBF and CTBF overlapped due to cyclic thermal fluctuations. A second notable weight loss phase in UBF, occurring around 375–400 °C, is predominantly linked to thermal degradation of biomass, including the breakdown of hemicellulose and cellulose structures[47]. Moreover, the substantial alterations in the thermal peak positions of CTBF indicate restructuring in the fiber surface chemistry, likely due to the formation of new chemical phases induced by Ca $(OH)_2$ treatment. Also, the minimized thermal degradation of CTBF is attributed to the encapsulation of fibers with calcium hydroxide on the surface[48]. Beyond 500 °C, TGA curves indicate negligible mass change and tend to exhibit asymptotic behavior.

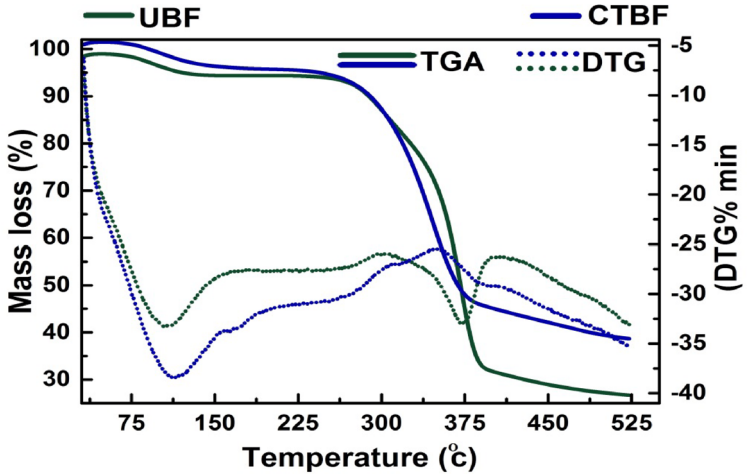

Fig. 8. TGA-DTG curves of untreated and chemically treated banana fiber.

Properties	$S.A_6$				
	$(C_{100}F_0)$	$(C_{95}F_5)$	$(C_{90}F_{10})$	$(C_{85}F_{15})$	$(C_{80}F_{20})$
Dry density (kN/m^3)	16.75	17.5	17.8	18.0	18.3
Moisture content (%)	19.5	18.5	18.3	18.1	18.0
Linear shrinkage (%)	6.35	6.24	6.39	6.59	6.85
Plasticity index (%)	19.1	18.6	17.9	17.4	16.9
Swell index (%)	30.4	28.1	27.9	26.5	25.1
Swell Pressure (kPa)	46.2	41.4	34.1	31.2	27.5

Table 5. Geotechnical results of geopolymer-soil at varying CGA-SF content.

Geotechnical characterization

A series of geotechnical tests was performed on geopolymer-stabilized soil incorporating various CGA–SF blend ratios. The corresponding geotechnical properties are presented in Table 5.

Consolidation

Soil compressibility (relative to equilibrium void ratio) for low-plasticity clay, CGA-SF-based alkaline stabilized soil, is plotted against effective stress. The variance in initial void ratio curves for both untreated soil and geopolymer-stabilized soils is presented graphically in Fig. 9. The trend of the void ratio plots illustrates the relationship between soil swelling behavior and the rate of applied seating load. During the early phase, untreated low-plasticity clay demonstrates a greater final void ratio compared to the alkaline-treated soil, as indicated by the e–log(σ) response. This is due to the existence of active moisture retention around the clay matrix and also being rich in silica and iron-illite compounds, effectively delaying the moisture infiltration, thus requiring a longer time to reach an equilibrium swelling stage[49,50]. The addition of CGA-SF-based geopolymer-stabilized soil aids in restricting the rate of void ratio effects (from 0.92 to 0.54); this marginal reduction may be due to the activation of the geopolymerization reaction in the clay composition, which adversely impacts the mineralogy. As the proportion of SF increases in place of CGA within the geopolymer blend, a significant reduction in volumetric expansion is observed. Notably, the combined incorporation of 20% SF and 80% CGA in the alkaline matrix results in a marked decrease in both void ratio and swelling across all geopolymer-stabilized soil compositions. Moreover, the drastic changes in and around the clay structure can also be substantially responsible for the drop in void ratio from 0.72 to 0.47 (20% SF-based geopolymer-soil). Through pozzolanic-ion consumption during active cementing gel formation, SF-based geopolymer stabilized surface particles may improve the interlocking bonding capacity of clay at low-effective stress applications[51,52]. Thus, in geopolymer-mixed soil, creating consistent cementitious coatings with a new morphology reduces compressible behavior and the rate of void ratio reduction.

Unconfined compressive strength (UCS)

The UCS measurements of geopolymer-stabilized soil incorporating varying dosages of pozzolanic materials within the alkaline binder are illustrated in Fig. 10, which highlights the combined influence of fiber, CGA, and SF on strength enhancement in low-plasticity clay. A partial replacement of CGA (100–90%) with SF (0–10%) initially slows the development of compressive strength, which may be attributed to the low pozzolanic activity of silica and alumina present in CGA-based systems. As the content of SF and CTBF increases, the strength performance of geopolymer-treated soil improves progressively. The denser and more cohesive matrix formation

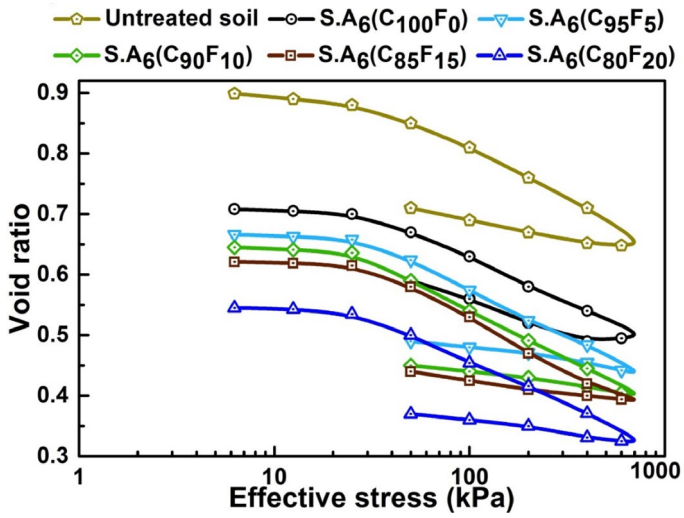

Fig. 9. Void ratio variations at different effective stresses for untreated and geopolymer-treated soils under varying CGA-SF dosages.

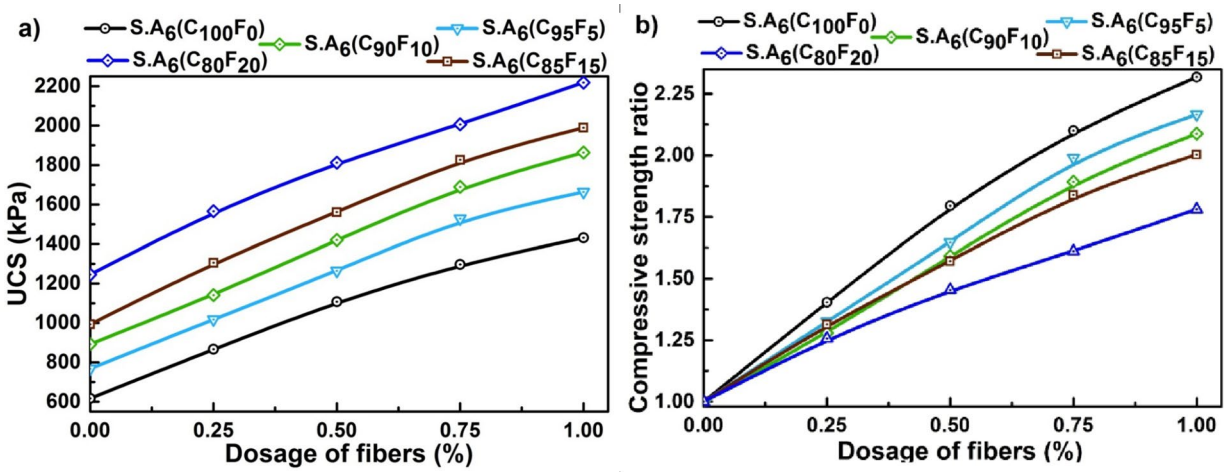

Fig. 10. Variation of **(a)** UCS and **(b)** Compressive strength ratio of geopolymer-CTBF-reinforced soil at varying CGA-SF dosage.

in the AAM-treated soil is likely due to the accelerated production of calcium and sodium silicate hydrate gels, which results from the higher availability of reactive silica provided by the SF. This strength gain (from 620 kPa to 1260 kPa) is linked to the active geopolymerization reaction between clay particles and pozzolanic products in the alkaline matrix, leading to the formation of a denser microstructure[53–55]. It is also interesting to note that the discrete CTBF inclusion effectively enhances the shear resistance power by bridging microcracks and improving load transfer between the gel matrix and soil particles, resulting in prolonging crack propagation and strengthening ductility. The results also show that increasing the CTBF (0% to 1%) improves soil shear strength from 1280 kPa ($SA_6C_{100}F_0$) to 2160 kPa ($SA_6C_{80}F_{20}$). The increasing UCS trends reveal strong interlock particle bonding between the fiber matrix and clay structures that indirectly benefit from the geopozzolanic reaction. Therefore, the cohesive strength of the geopolymer-stabilized soil is directly influenced by the combined presence of SF and CTBF.

Figure 10(b) illustrates the compressive strength ratio (CSR) behavior of geopolymer soil reinforced with CTBF across different CGA–SF mix proportions. The CSR-based compressive strength analysis highlights the role of CTBF in enhancing confinement effects, primarily through increased interparticle friction and improved bonding within the alkaline-treated matrix, resulting in greater density and stiffness. When the soil matrix is stabilized using 100% CGA (with no SF), the CTBF–geopolymer system attains a CSR range of approximately 2.0–2.5. Similar CSR values (2.2–3.0) have been reported by Park[56] and Bekhiti et al.[57] for waste rubber fiber-reinforced cementitious materials. In comparison, for kaolinite clay treated with 1% glass fiber and 1% polypropylene fiber, Maher and Ho[58] and Rios et al.[59] reported a maximum CSR of 1.2. As SF partially replaces CGA (up to 20%) in the mix, the CSR of the CTBF–geopolymer system tends to align with the corresponding

compressive strength, showing a value around 1.65. The fiber matrix develops mechanical interlocking and a $Ca(OH)_2$ rich interfacial zone that increases the bond density within the pozzolanic soil composite; stereomicroscopy reveals a grooved fiber network and AAM-hardened paste deposited along the cracks, while FTIR shows stronger Si-O-Al molecular bond linkages. These attributes can increase overall lateral restraint and stress transfer under axial load. It is important to note that increasing CTBF dosage beyond 0.6% and SF content above 10% results in a modest improvement in the shear strength ratio. The increased dosage of the SF in the alkaline binder compound actively enhances the soil interbonding density between CTBF-geopolymer soils. Additionally, the addition of SF is beneficial to CGA-based geopolymer soil, as it actively produces calcium silicate gel from its available silica-calcium compounds, resulting in low soil moisture attraction around the CTBF-clay particles. This forms a dense bridge effect, characterized by strong particle-holding efficiency, and enhances the compressive shear resistance during geopolymerization. Moreover, the CTBF are mobilized later and contribute a lesser proportion of the total load; therefore, even while relative UCS still increases, the CSR increment per fiber dosage decreases when SF exceeds about 10% because the matrix becomes denser and stiffer, reducing initial crack density and slip planes. The rough surface of CTBF strongly holds the pozzolanic encapsulated clay particles, which are difficult to reorient, and can improve interlocking friction resistance against loading[60,61]. Thus, the active formation of geopolymerization in the SF-based CTBF-geopolymer soil can strengthen the ultimate pulling stress under strong linkage effects.

California bearing ratio (CBR)

The influence of pozzolanic precursors and alkaline activators on the performance enhancement of subgrade soil was analyzed through penetration resistance measurements. The soaked CBR tests will indirectly provide a clue to the efficiency of subgrade geomaterials under the long-term effect at different CTBF-CGA-SF proportions in the geopolymer-soil mixture. Figure 11(a) shows the variation in soaking CBR values for untreated soil and CTBF-reinforced geopolymer mixed soil. Under CGA replacement with SF Geopolymer addition improved the penetration resistance of the soil improved from 2.28% to 5.87%. The CBR improvement likely results from geopozzolanic activation during soaking[62]. The synthesis of SF between the CGA-fiber matrices induces an active multivalent cationic growth that minimizes clay compressibility[63–66]. Moreover, the formation of dense pozzolanic compounds within the silica-rich matrix significantly enhances the bonding of flocculated particles, leading to greater penetration-locking density. It is important to highlight that the combined use of 20% SF and 80% CGA in the alkaline binder results in a substantial improvement in penetration resistance, along with minimal swelling across all geopolymer-based CGA/SF mixtures. Additionally, Fig. 11(b) presents the soaked CBR-derived resilient modulus values, which serve as a reliable indicator of subgrade soil stiffness. To minimize data clustering, only selected results for CTBF–geopolymer-stabilized soil with CGA: SF ratios of 100:0, 90:10, and 80:20 are shown. The resilient modulus outcomes highlight the interaction between soil penetration resistance and specific slag content, particularly under higher PLF dosages in the treated soil. It reveals that the CTBF and SF proportions in CGA-based geopolymer composites play a key role in increasing subgrade strength and bearing resistance under regulated swell-shrinkage behavior. The resilient modulus trend of soil is similar to that of CBR penetration with the addition of binder and fiber to the soil. A significant increase in the CBR-based resilient modulus of geopolymer-stabilized subgrade soils was observed beyond 0.5% CTBF reinforcement, particularly within the 0.2–0.4% PLF range when SF content exceeded 10% in the alkaline binder. Hence, geopolymerization driven by pozzolanic gels contributes to the formation of a bonded network around the CTBF–geopolymer–soil matrix, improving penetration resistance.

Comparative efficiency of SVM-based predictive models

Figures 12 and 13 illustrate the regression plot between the measured data and model predictions, illustrating the predictive strength of SVM-based modeling. In this regard, the residual error and training-testing errors are visualized to determine the robustness of the SVM-based models. It can be observed that the SVM optimization exhibits a substantial impact on the predicted outputs. When optimized through grid search methods, the testing

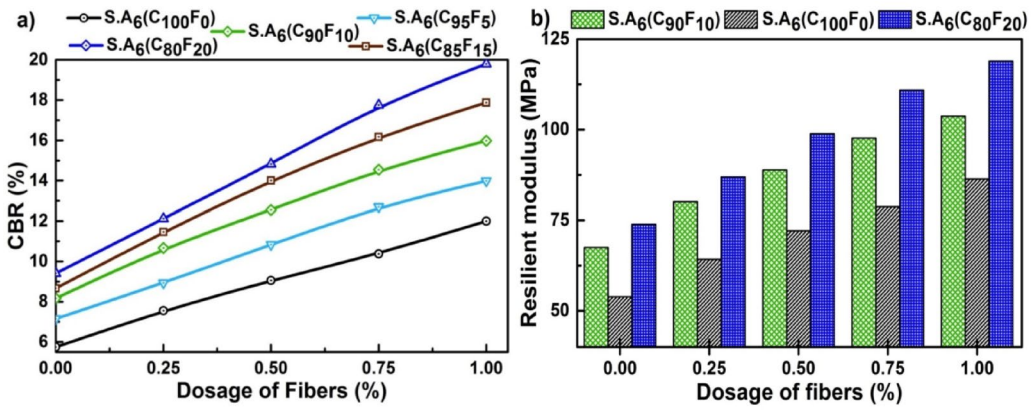

Fig. 11. Effect of CGA–SF proportions on **(a)** soaked CBR values and **(b)** resilient modulus of CTBF-reinforced geopolymer soil.

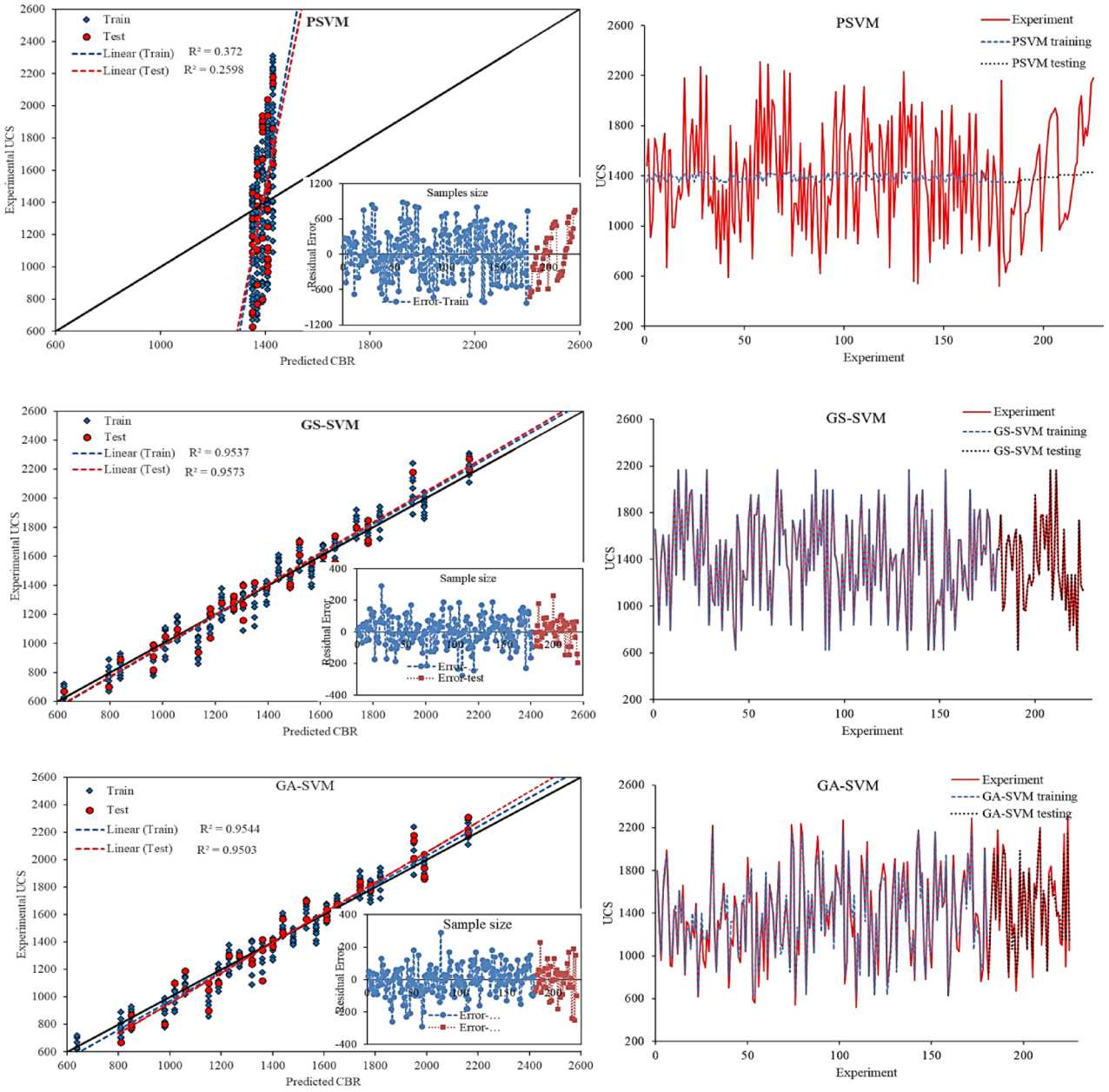

Fig. 12. Prediction results of UCS corresponding to: **(a)** SVM, **(b)** GS-SVM, and **(c)** GA-SVM approaches, along with the error measurements.

R^2 values yielded from the SVM models are improved by 270% and 220% (for UCS and CBR), respectively. It is noteworthy to mention that these improvements are also achieved by attaining R^2 of 0.95 (for UCS) and 0.965 (for CBR) in the GA approach, which validates the high efficiency of both optimization approaches.

Error area analysis

Error areas are another type of graphical analysis of uncertainty while considering predicted data. The difference between error area analysis and prediction error analysis (shown in Figs. 11 and 12, respectively) lies in the type of associated uncertainty. By propagating uncertainty through the input data before prediction, the corresponding error regions are identified. In contrast, the prediction error results in the aforementioned figures show the yielded error after prediction using the developed model. As a result, this uncertainty analysis introduces variability into the dataset, facilitating the evaluation of the models' generalization to unseen data.

To perform error area analysis, the standard deviation of the input entries is extended using a 95% confidence interval (CI), represented by the shaded regions. Broader error areas indicate less prediction certainty, while narrower areas imply more certainty. Moreover, Figs. 13 and 14 illustrate the error area analysis conducted during the training and testing stages of the GS-SVM and GA-SVM models for predicting strength characteristics. Evidently, the training of the models with deviated inputs is more certain. In contrast, the testing phase is highly

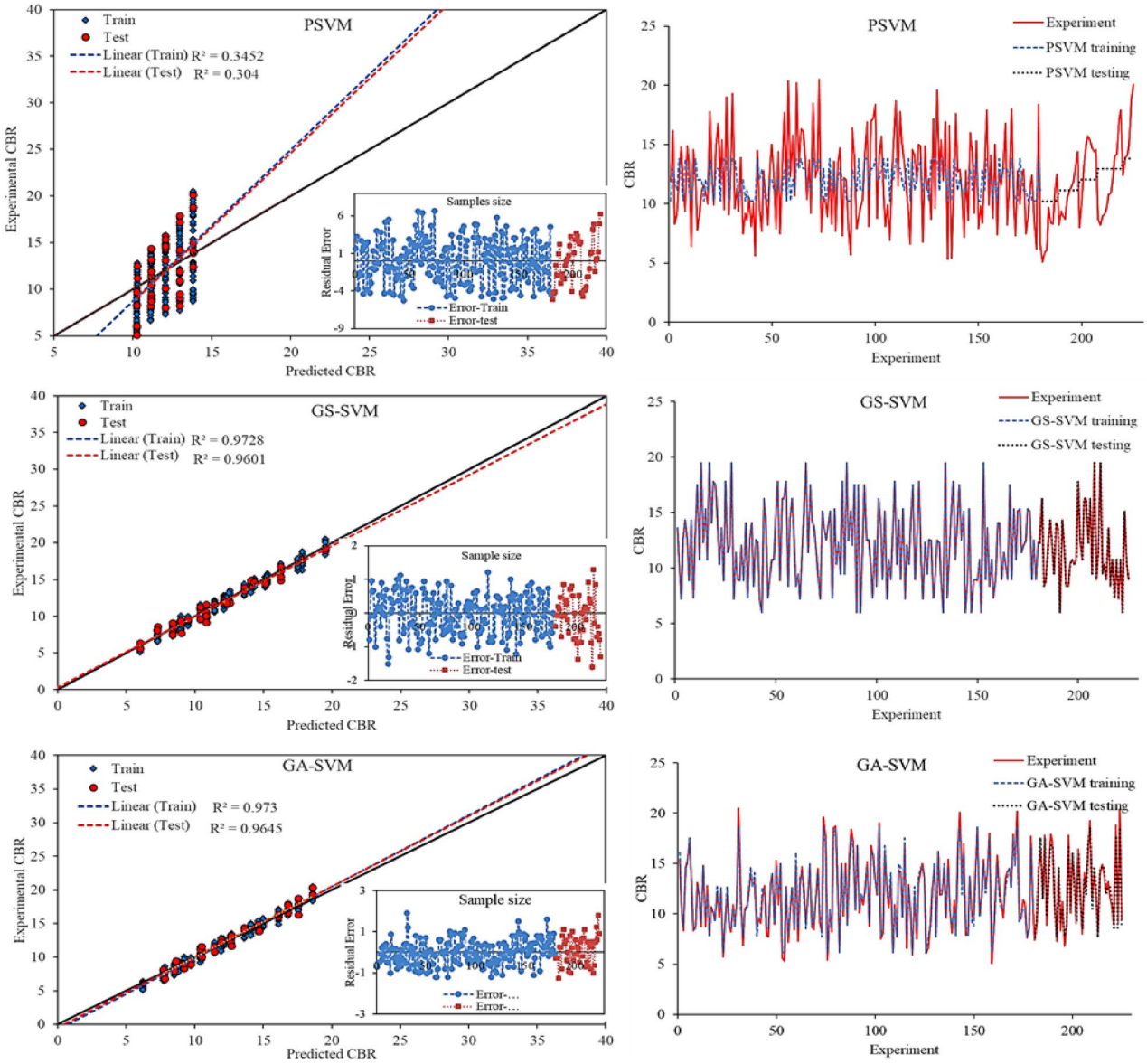

Fig. 13. Prediction results of CBR corresponding to **(a)** SVM, **(b)** GS-SVM, and **(c)** GA-SVM, along with the error measurements.

sensitive to inputs with large standard deviations. Noticeably, the regression fit results for the training stage yielded R^2 of 0.9728 and 0.973for for GS-SVM and GA-SVM, respectively. However, the testing performance showed a slight improvement for the GA-SVM model, with R^2 increasing from 0.9601 (GS-SVM) to 0.9645 (GA-SVM). These marginal differences, although not clearly visible in Figs. 11 and 12, indicate the influence of optimization through the Genetic algorithm.

Hence, the inclusion of such error area analysis better highlights the importance of these tasks. Figures 14 and 15 show encircled areas in the testing plots depicting differences between the two algorithms and their predictive values. This observation further underscores the importance of error analysis with confidence intervals (CIs) compared to common regression plots. Thus, it facilitates the identification of models demonstrating robust performance.

Comparative effects of input variables on the predicted output

One of the major advantages of predictive modelling lies in its ability to determine how input variables influence output parameters. However, previous studies have often lacked a clear representation of the relative significance and ranking of these variables. The magnitude of such influences can be accurately evaluated with the help of sensitivity analysis techniques, including feature importance and explainable AI approaches. Among these, SHAP (SHapley Additive exPlanations) provides a modern framework for quantifying the individual effects of input variables on model predictions. This technique offers both global insights, comparable to Sobol sensitivity

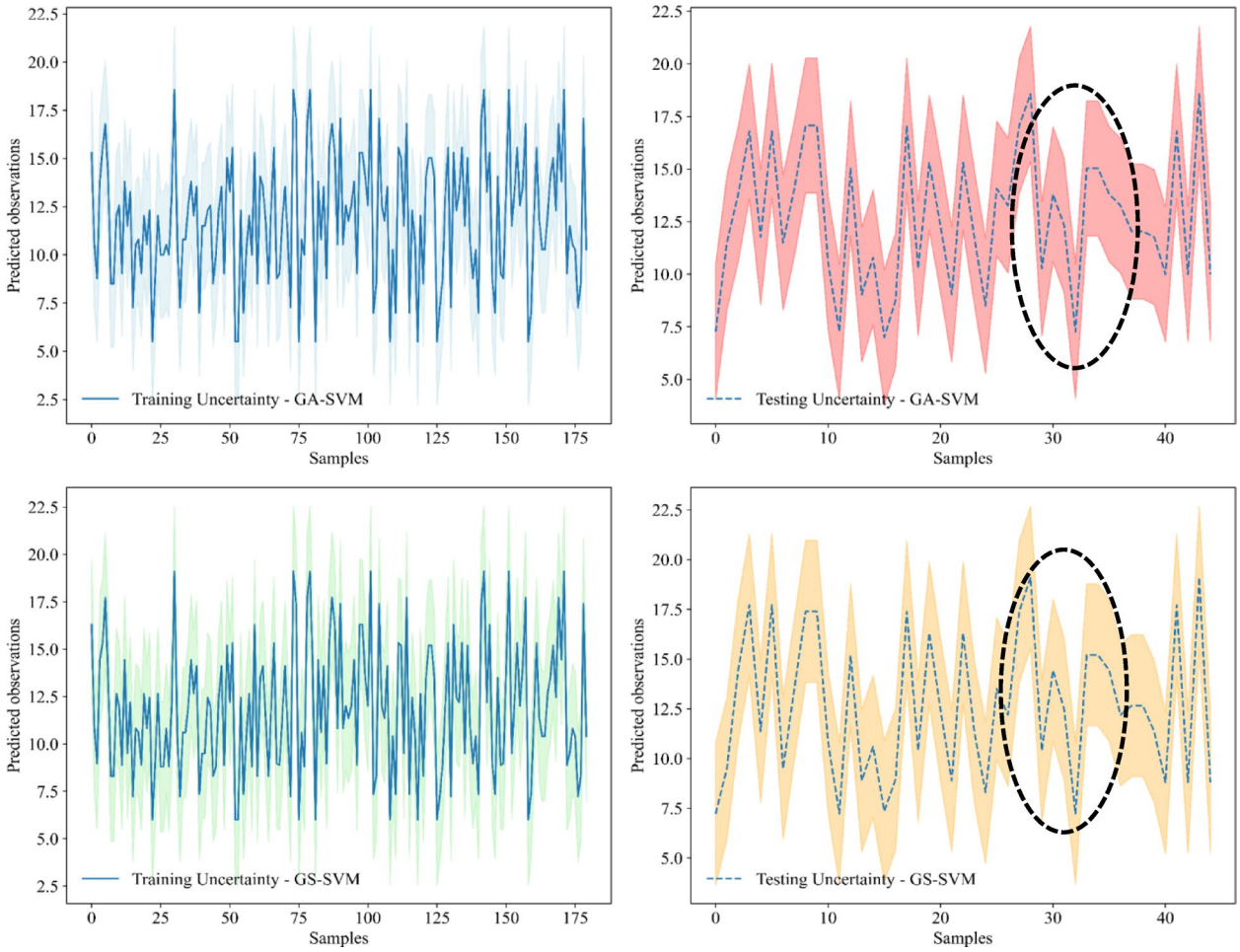

Fig. 14. Error area analysis during training and testing of GA-SVM and GS-SVM for predicting CBR with a 95% confidence interval.

analysis, and local interpretability. Additionally, the SHAP values quantify the relative impact of each input feature on the predicted output, thereby supporting a deeper understanding of both local and global model behaviour. The SHAP-based sensitivity results for the optimized SVM model predictions are illustrated in Fig. 16.

It should be noted that, despite the previous model analysis, the sensitivity results obtained from both GA-SVM and GS-SVM are almost identical. For brevity, only the GA-SVM results are presented herein. The analysis reveals that BF is the governing input parameter, affecting the output more than twice as strongly as the other variables. In contrast, the predictive contributions of CGA and SF are almost identical. As shown earlier (pair plots in Figs. 3 and 4), it is pertinent to mention that CGA and SF exhibit a strong negative relationship, which explains their similar effects on the output. On the contrary, BF has no significant correlation with the remaining input variables. These observations suggest that the variation in BF content would significantly alter the final strength values, given the current dosage and experimental plan. Furthermore, the influence of the input variables on the prediction of each output parameter is largely consistent. Each point in the SHAP plot represents the effect of a variable on individual data entries. Although the order of variable importance can be expressed as BF > CGA ≥ SF, the SHAP values for CBR prediction are observed to be more scattered. This observation indicates that the input variables exert a greater influence on CBR predictions in contrast to UCS. Hence, the measurement and preprocessing of CBR data require greater precision to minimize uncertainty in model predictions.

It is essential to validate the model-derived insights from the SHAP analysis using experimental evidence. The SHAP plots (Fig. 16) clearly identify BF as the most influential variable, where increased fibre content consistently leads to higher predicted UCS and CBR values. This observation aligns closely with the experimental results shown in Figs. 10a and 11a, where the inclusion of CTBF from 0% to 1% results in the most significant and consistent increase in the strength characteristics across all geopolymer-stabilized soil compositions. Furthermore, the SHAP analysis indicates a positive influence of SF and a negative influence of CGA on strength, which is directly corroborated by the experimental data. For any given fibre dosage in Figs. 10 and 11, the curves corresponding to higher SF content (e.g., $SA_6(C_{80}F_{20})$) consistently lie above those with lower SF content (e.g., $SA_6(C_{10}0F_0)$), indicating superior strength performance. This strong correlation between the SHAP-based

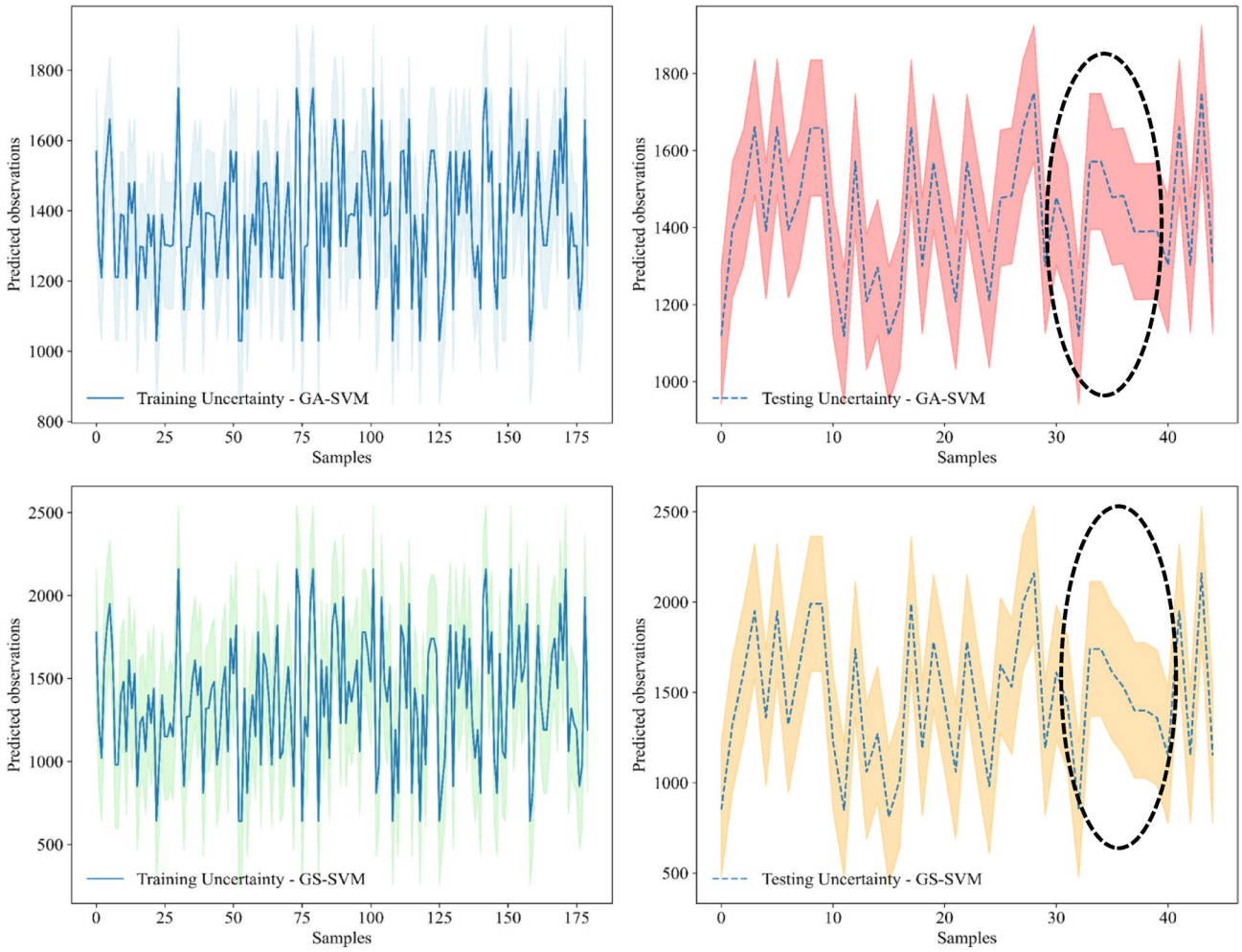

Fig. 15. Error area analysis during training and testing of GA-SVM and GS-SVM for predicting UCS with a 95% confidence interval.

sensitivity analysis and laboratory observations confirms that the optimized SVM model accurately captures the hierarchical influence of the input parameters on the geomechanical behavior of the stabilized low-plasticity clay.

Summary and conclusions

This research investigates the combined influence of CTBF reinforcement on low-plasticity clay stabilized with coal gangue ash and silica fume-based geopolymers. The influence of CGA-SF proportions on consolidation and CTBF reinforcement on geomechanical strength performance indicators (compressive strength, shear strength ratio, CBR, and resilient modulus) of geopolymer stabilized low-plasticity clay was investigated. Furthermore, an optimal SVM model was developed to analyze the geomechanical strength behavior, including compressive shear and penetration resistance, of CTBF-geopolymer soil at various CGA-SF dosages. The key findings of this research are outlined in the conclusion section that follows.

- The growth of geopolymeric cementitious gel around the CTBF-clay matrices is observed after geopolymer treatment (soil surface cracks and pores filling and forming a hardened geopolymer thin layer). Moreover, the addition of discrete CTBF alkaline soil has formed a spatial groove clay network structure, enhancing the soil-tensile interfacial density under strong interlocking friction.
- The growth of new molecular bonds (Si-O-Si and Si-O-Al) linked to activating geopolymerization reactions. Also, in the CTBF, the C = O and $-CH_2$ alkene-lignin group is identified, corresponding to the carbonation reaction. In TGA/DTG measurement, the mass loss fraction of CTBF decreases compared to UBF, overcoming the early biodegradability of the material.
- At an optimal blend ratio of 80:20 (CGA to SF), the geopolymer-treated soil demonstrates improved volumetric stability by reducing the equilibrium void ratio by up to 68%. CTBF–geopolymer composites also show enhanced penetration resistance and subgrade resilient modulus, achieving a 68% increase in CBR strength at the ideal fiber reinforcement level of 1%.

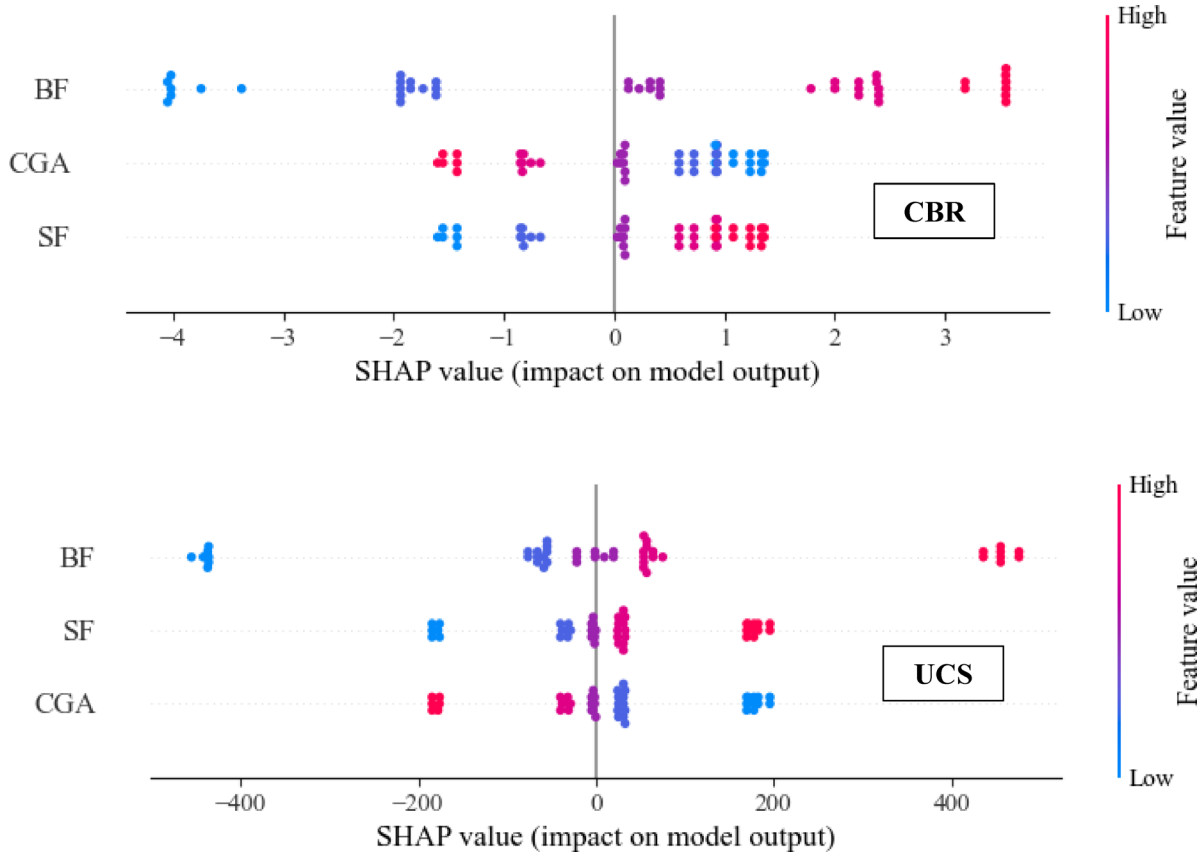

Fig. 16. Variable importance analysis in the prediction of UCS and CBR.

- The shear strength ratio of geopolymer-treated soil decreases significantly when CGA is partially replaced with SF in the alkaline binder. Moreover, CTBF enhances the confinement bonding with dense cementitious layers surrounding it, achieving higher durability by preventing early biodegradation.
- The improvement in UCS was notable when CTBF, CGA, and SF were combined in the alkaline soil stabilizer. Additionally, the proposed SV model for geomechanical strength, in terms of UCS and CBR, exhibits the lowest error percentages (< 10%) regardless of CGA: SF content.
- The regression fit results of training for both GS-SVM and GA-SVM were R^2 of 0.9728 and 0.973, 536, respectively. However, the testing results were slightly higher in the case of GA-SVM during testing, with an increase from R^2 of 0.9601 for GS-SVM to R^2 of 0.9645 for GA-SVM.
- According to SHAP analysis, the order of variable importance can be put as BF > CGA ≥ SF; however, during the prediction of CBR values, the SHAP values are observed to be more scattered. This observation indicates that the inputs affect the prediction course of CBR comparatively more than the UCS.

Data availability

The datasets used and/or analysed during the current study are available from the corresponding author on reasonable request.

Received: 3 September 2025; Accepted: 11 November 2025
Published online: 23 December 2025

References

1. Jangde, H., Khan, F. & Ghaffar, A. Exploring the Correlation Between Compressive Strength and Hydraulic Conductivity in Soft Soil with Metakaolin as a Stabilizing Agent: An Experimental Study. in *Int. Conf. Interdiscip. Approaches Civ. Eng. Sustain. Dev.* 79–89Springer, (2023).
2. Luo, Z. & Zhang, B. Effect of humic acid and fulvic acid on mechanical and durability properties of geopolymer stabilized soft soil. *Constr. Build. Mater.* **409**, 133875 (2023).
3. Yuan, B. et al. Dynamic behavior and deformation of calcareous sand under Cyclic loading. *Soil. Dyn. Earthq. Eng.* **199**, 109730 (2025).
4. Jiang, N., Wang, C., Wu, Q. & Li, S. Influence of structure and liquid limit on the secondary compressibility of soft soils. *J. Mar. Sci. Eng.* **8**, 627 (2020).
5. Nagaraj, T. S. & Pandian, N. S. Narasimha Raju, P. S. R. Compressibility behaviour of soft cemented soils. *Geotechnique* **48**, 281–287 (1998).

6. Zhu, G., Zhu, L. & Yu, C. Rheological properties of soil: A review. in *IOP Conf. Ser. Earth Environ. Sci.* **64**, 12011. IOP Publishing (2017).
7. Chen, T. & Zhang, G. Centrifuge modeling of pile-supported embankment on soft soil base for highway widening. *Soils Found.* **64**, 101422 (2024).
8. Rosli, N., Saad, R., Rahman, N. & Ismail, N. A. Soft soils: A study on their electrical resistivity values and geotechnical properties (porosity, SPT and particle size distribution). (2020).
9. Pedarla, A., Puppala, A. J., Hoyos, L. R. & Chittoori, B. Evaluation of swell behavior of expansive clays from internal specific surface and pore size distribution. *J. Geotech. Geoenvironmental Eng.* **142**, 04015080 (2015).
10. Niu, W. et al. Cementitous material based stabilization of soft soils by stabilizer: feasibility and durabiliy assessment. *Constr. Build. Mater.* **425**, 136046 (2024).
11. Ouedraogo, K. A. J., Aubert, J. E., Tribout, C. & Escadeillas, G. Is stabilization of Earth bricks using low cement or lime contents relevant? *Constr. Build. Mater.* **236**, 117578 (2020).
12. Rangaswamy, K. & Mohan, R. P. Nano-Chemical Stabilization of Soft Soil as a Paved Subgrade Material. in *Int. Symp. Constr. Resour. Environ. Sustain. Technol.* 131–141 (Springer, 2023).
13. Yuan, B. et al. Effects of particle size on properties of engineering muck-based geopolymers: optimization through Sieving treatment. *Constr. Build. Mater.* **492**, 142967 (2025).
14. Yuan, B. et al. Mechanical and microstructural properties of recycling granite residual soil reinforced with glass fiber and liquid-modified Polyvinyl alcohol polymer. *Chemosphere* **286**, 131652 (2022).
15. Ashfaq, M., Moghal, A. A. B, Basha, B. M. & Moghal, A. A. B. Carbon footprint analysis on the expansive soil stabilization techniques. *IFCEE ASCE* **2021**, 213–222 (2021).
16. Moghal, A. A. B., Ashfaq, M., Al-Shamrani, M. A. & Al-Mahbashi, A. Effect of heavy metal contamination on the compressibility and strength characteristics of chemically modified semiarid soils. *J. Hazard. Toxic. Radioact Waste.* **24**, 1–10 (2020).
17. Li, Y., Li, J., Cui, J., Shan, Y. & Niu, Y. Experimental study on calcium carbide residue as a combined activator for coal gangue geopolymer and feasibility for soil stabilization. *Constr. Build. Mater.* **312**, 125465 (2021).
18. Snehasree, N., Nuruddin, M. & Moghal, A. A. B. Critical appraisal of coal gangue and activated coal gangue for sustainable engineering applications. *Appl. Sci.* **15**, 9649 (2025).
19. Gaddam, A. G., Amulya, G., Bind, A. & Yamsani, S. K. Effective utilization of coal gangue for stabilizing black cotton soil: geotechnical performance and microstructural insights. *Transp. Infrastruct. Geotechnol.* **12**, 1–22 (2025).
20. Tang, T., Wang, Z., Chen, L., Wu, S. & Liu, Y. Opportunities, challenges and modification methods of coal gangue as a sustainable soil conditioner—a review. *Environ. Sci. Pollut Res.* **31**, 58231–58251 (2024).
21. Wang, X. et al. Geopolymerization of coal gangue via alkali-Activation: dependence of mechanical properties on alkali activators. *Buildings* **14**, 1–19 (2024).
22. Ashfaq, M., Moghal, A. A. B. & Basha, B. M. The sustainable utilization of coal gangue in geotechnical and geoenvironmental applications. *J. Hazard. Toxic. Radioact Waste.* **26**, 1–16 (2022).
23. Yan, P. et al. Laboratory tests, field application and carbon footprint assessment of cement-stabilized pure coal solid wastes as pavement base materials. *Constr. Build. Mater.* **366**, 130265 (2023).
24. Bualuang, T. et al. Utilization of dumped coal Ash from power-plant landfills for carbon footprint reduction in sustainable pavement base construction. *Constr. Build. Mater.* **441**, 137462 (2024).
25. Ashfaq, M. & Moghal, A. A. B. Cost and carbon footprint analysis of flyash utilization in earthworks. *Int. J. Geosynth Gr Eng.* **8**, 21 (2022).
26. Gajurel, A., Chittoori, B., Mukherjee, P. S. & Sadegh, M. Machine learning methods to map stabilizer effectiveness based on common soil properties. *Transp. Geotech.* **27**, 100506 (2021).
27. Tamassoki, S., Daud, N. N. N., Wang, S. & Roshan, M. J. CBR of stabilized and reinforced residual soils using experimental, numerical, and machine-learning approaches. *Transp. Geotech.* **42**, 101080 (2023).
28. Ashfaq, M. & Moghal, A. A. B. Influence of lime and coal gangue on the CBR behavior of expansive soil. Sustain. Civ. Infrastructures (Springer International Publishing, doi:https://doi.org/10.1007/978-3-030-80155-7_7 (2021).
29. Ashfaq, M., Lal, M. H., Moghal, A. A. B. & Murthy, V. R. Carbon footprint analysis of coal gangue in geotechnical engineering applications. *Indian Geotech. J.* **50**, 646–654 (2020).
30. Amin, M. N. et al. Prediction of strength and CBR characteristics of chemically stabilized coal gangue: ANN and random forest tree approach. *Mater. (Basel).* **15**, 4330 (2022).
31. Syarif, I., Prugel-Bennett, A. & Wills, G. SVM parameter optimization using grid search and genetic algorithm to improve classification performance. *TELKOMNIKA (Telecommunication Comput. Electron. Control.* **14**, 1502–1509 (2016).
32. Ly, H. B., Nguyen, M. H. & Pham, B. T. Metaheuristic optimization of Levenberg–Marquardt-based artificial neural network using particle swarm optimization for prediction of foamed concrete compressive strength. *Neural Comput. Appl.* **33**, 17331–17351 (2021).
33. Mohamad, E. T., Armaghani, J. & Momeni, D. Alavi Nezhad Khalil Abad, S. V. Prediction of the unconfined compressive strength of soft rocks: a PSO-based ANN approach. *Bull. Eng. Geol. Environ.* **74**, 745–757 (2015).
34. Biswas, R. et al. Efficient soft computing techniques for the prediction of compressive strength of geopolymer concrete. *Comput. Concr.* **28**, 221–232 (2021).
35. Kurani, A., Doshi, P., Vakharia, A. & Shah, M. A comprehensive comparative study of artificial neural network (ANN) and support vector machines (SVM) on stock forecasting. *Ann. Data Sci.* **10**, 183–208 (2023).
36. C618–14, A. Standard Specification for Coal Fly Ash and Raw or Calcined Natural Pozzolan for Use in Concrete. at. (2014).
37. C989, A. ASTM C989 / C989M-16 standard specification for slag cement for use in concrete and mortars. American Society for Testing and Materials, West Conshohocken, PA. 16. ASTM 1, 1–6. (2016).
38. Syed, M., GuhaRay, A. & Garg, A. Performance evaluation of lime, cement and alkali-activated binder in fiber-reinforced expansive subgrade soil: A comparative study. *J Test. Eval.* **51**, 3054–3077 (2021).
39. Miller, S. A., Srubar, W. V., Billington, S. L. & Lepech, M. D. Integrating durability-based service-life predictions with environmental impact assessments of natural fiber-reinforced composite materials. *Resour. Conserv. Recycl.* **99**, 72–83 (2015).
40. Syed, M., Jalal, F. E., Shoeb, M. D., Alshawmar, F. & Abdeldjouad, L. Subgrade strength indicator model for geopolymerized soil reinforced with discrete fiberglass: A GEP approach. *Arab. J. Sci. Eng.* https://doi.org/10.1007/s13369-025-10701-0 (2025).
41. IRC:37-2018. Guidelines for the design of flexible pavements. IRC:37-2018 1–94. (2018).
42. Chen, W., Hasanipanah, M., Nikafshan Rad, H., Jahed Armaghani, D. & Tahir, M. M. A new design of evolutionary hybrid optimization of SVR model in predicting the blast-induced ground vibration. *Eng. Comput.* **37**, 1455–1471 (2021).
43. Mir, S. S., Hasan, S. M. N., Hossain, M. J. & Hasan, M. Chemical modification effect on the mechanical properties of Coir fiber. *Eng. J.* **16**, 73–83 (2012).
44. Syed, M., Ahuja, M., Jambholkar, A. R. & GuhaRay, A. Laboratory Investigation on Fiber-Reinforced Expansive Subgrade Soil Stabilized with Alkali Activated Binder: A Reliability-Based Perspective. in *Geo-Congress 2022* 241–250 (2022).
45. Cesar dos Santos, J. et al. Mechanical properties of epoxy banana fibre composite trated with sodium carbonate. (2016). at https://www.researchgate.net/publication/307571059
46. Komal, U. K., Verma, V., Ashwani, T., Verma, N. & Singh, I. Effect of chemical treatment on Thermal, mechanical and degradation behavior of banana fiber reinforced polymer composites. *J. Nat. Fibers.* **17**, 1026–1038 (2020).

47. Ferreira, S. R., Silva, F. D. A. & Lima, P. R. L. Toledo Filho, R. D. Effect of fiber treatments on the Sisal fiber properties and fiber-matrix bond in cement based systems. *Constr. Build. Mater.* **101**, 730–740 (2015).
48. Varma, A. K. & Mondal, P. Physicochemical characterization and pyrolysis kinetic study of sugarcane Bagasse using thermogravimetric analysis. *J. Energy Resour. Technol.* **138**, 1–11 (2016).
49. Kayabali, K. & Yaldiz, Ö. Investigation of the relationship between swell pressure and shrinkage limit. *Electron. J. Geotech. Eng.* **17 P**, 2313–2325 (2012).
50. Soltani, A., Deng, A. & Taheri, A. Swell–compression characteristics of a fiber–reinforced expansive soil. *Geotext. Geomembranes.* **46**, 183–189 (2018).
51. Meisina, C. Swelling-shrinking properties of weathered clayey soils associated with shallow landslides. *Q. J. Eng. Geol. Hydrogeol.* **37**, 77–94 (2007).
52. Chittoori, B. C. S., Moghal, A. A. B., Pedarla, A. & Al-Mahbashi, A. M. Effect of unit weight on porosity and consolidation characteristics of expansive clays. *J. Test. Eval.* **45**, 94–104 (2017).
53. Ahmad, S., Shah Alam Ghazi, M., Syed, M. & Al-Osta, M. A. Utilization of fly Ash with and without secondary additives for stabilizing expansive soils: A review. *Results Eng.* **22**, 102079 (2024).
54. Alsafi, S., Farzadnia, N., Asadi, A. & Huat, B. K. Collapsibility potential of gypseous soil stabilized with fly Ash geopolymer; characterization and assessment. *Constr. Build. Mater.* **137**, 390–409 (2017).
55. Syed, M., GuhaRay, A., Chukka, S. K. & Ahmad, S. A laboratory investigation and numerical modeling on fiber reinforced lime and alkaline binder stabilized pavement subgrade soil. *Case Stud. Constr. Mater.* **20**, e03000 (2024).
56. Park, S. S. Unconfined compressive strength and ductility of fiber-reinforced cemented sand. *Constr. Build. Mater.* **25**, 1134–1138 (2011).
57. Bekhiti, M., Trouzine, H. & Rabehi, M. Influence of waste tire rubber fibers on swelling behavior, unconfined compressive strength and ductility of cement stabilized bentonite clay soil. *Constr. Build. Mater.* **208**, 304–313 (2019).
58. Maher, M. H. & Ho, Y. C. Mechanical properties of Kaolinite/Fiber soil composite. *J. Geotech. Eng.* **120**, 1381–1393 (1995).
59. Rios, S., Ramos, C. & Rodrigues, C. Mechanical and durability properties of a soil stabilised with an alkali-activated cement. *Eur. J. Environ. Civ. Eng.* **8189**, 1–23 (2017).
60. Tang, C., Shi, B., Gao, W., Chen, F. & Cai, Y. Strength and mechanical behavior of short polypropylene fiber reinforced and cement stabilized clayey soil. *Geotext. Geomembranes.* **25**, 194–202 (2007).
61. Mazhar, S. & Guharay, A. Stabilization of expansive clay by fibre-reinforced alkali-activated binder: an experimental investigation and prediction modelling. *Int. J. Geotech. Eng.* **15**, 1–17 (2020).
62. Syed, M., Moghal, A. A. B. & Chittoori, B. Reliability Analysis of Polyvinyl Alcohol Fiber-Reinforced Soft Subgrade Soil Treated with Lime and Alkali Activated Stabilizer: A Comparative Study. in *Geo-Congress 2023* 422–432 ASCE, (2023).
63. Shahbazi, M., Rowshanzamir, M., Abtahi, S. M. & Hejazi, S. M. Optimization of carpet waste fibers and steel slag particles to reinforce expansive soil using response surface methodology. *Appl. Clay Sci.* https://doi.org/10.1016/j.clay.2016.11.027 (2017).
64. Moghal, A. A. B., Chittoori, B. C. S. & Basha, B. M. Effect of fibre reinforcement on CBR behaviour of lime-blended expansive soils: reliability approach. *Road. Mater. Pavement Des.* **19**, 690–709 (2018).
65. Pourakbar, S. & Huat, B. K. A review of alternatives traditional cementitious binders for engineering improvement of soils. *Int. J. Geotech. Eng.* **11**, 206–216 (2017).
66. Priyadharshini, P., Ramamurthy, K. & Robinson, R. G. Excavated soil waste as fine aggregate in fly ash based geopolymer mortar. *Appl. Clay Sci.* **146**, 81–91. https://doi.org/10.1016/j.clay.2017.05.038 (2017).

Acknowledgements

The authors gratefully acknowledge the support provided by the Deanship of Research at King Fahd University of Petroleum and Minerals (KFUPM) for facilitating this study. The authors gratefully acknowledge the funding support from Interdisciplinary Research Center for Construction and Building Materials (IRC-CBM), KFUPM, for the project grant INCB2515.

Author contributions

Mazhar Syed : Methodological Framework, Research Execution, and Writing – Original DraftMohammed Ashfaq : Idea Development, Supervision, and Critical Review of the ManuscriptBabak Jamhiri : Software Implementation, Analytical Modeling..Umair Ali: Project administration, Resources, Supervision, Review, and editing. Fazal E. Jalal: Conceptualization, Research Execution, Review, writing & editing.

Declarations

Competing interests

The authors declare no competing interests.

Additional information

Correspondence and requests for materials should be addressed to U.A. or F.E.J.

Reprints and permissions information is available at www.nature.com/reprints.

Publisher's note Springer Nature remains neutral with regard to jurisdictional claims in published maps and institutional affiliations.